

Magnetic fields and Sunyaev-Zel'dovich effect in galaxy clusters

Rajesh Gopal

*CAPSS, Bose Institute,
Block - EN, Sector V, Salt Lake city, Kolkata - 700091, West Bengal, India
E-mail: rgpune@gmail.com*

Suparna Roychowdhury

*Dept. of Physics, St. Xavier's College (Autonomous),
30, Park Street, Kolkata - 700016, West Bengal, India
E-mail: suparna.roychowdhury@gmail.com*

ABSTRACT: In this work we study the contribution of magnetic fields to the Sunyaev Zeldovich (SZ) effect in the intracluster medium. In particular we calculate the SZ angular power spectrum and the central temperature decrement. The effect of magnetic fields is included in the hydrostatic equilibrium equation by splitting the Lorentz force into two terms – one being the force due to magnetic pressure which acts outwards and the other being magnetic tension which acts inwards. A perturbative approach is adopted to solve for the gas density profile for weak magnetic fields ($\leq 4\mu\text{G}$). This leads to an enhancement of the gas density in the central regions for nearly radial magnetic field configurations. Previous works had considered the force due to magnetic pressure alone which is the case only for a special set of field configurations. However, we see that there exists possible sets of configurations of ICM magnetic fields where the force due to magnetic tension will dominate. Subsequently, this effect is extrapolated for typical field strengths ($\sim 10\mu\text{G}$) and scaling arguments are used to estimate the angular power due to secondary anisotropies at cluster scales. In particular we find that it is possible to explain the excess power reported by CMB experiments like CBI, BIMA, ACBAR at $\ell > 2000$ with $\sigma_8 \sim 0.8$ (WMAP 5 year data) for typical cluster magnetic fields. In addition we also see that the magnetic field effect on the SZ temperature decrement is more pronounced for low mass clusters ($\langle T \rangle \sim 2 \text{ keV}$). Future SZ detections of low mass clusters at few arc second resolution will be able to probe this effect more precisely. Thus, it will be instructive to explore the implications of this model in greater detail in future works.

KEYWORDS: Cosmology, Galaxies, clusters, Magnetic field.

Contents

1. Introduction	1
2. Formulation	2
2.1 Dark matter density profile	3
2.2 Universal temperature profile	4
2.3 Hydrostatic equilibrium of gas in presence of magnetic field	4
2.3.1 Density profile in the absence of magnetic field	4
2.3.2 Density profile in the presence of magnetic field	5
3. Compton y-parameter and central SZ decrement	7
4. Angular power spectrum	8
5. Results & Discussion	9
5.1 Magnetic field configurations and Lorentz force	9
5.2 Density profiles	10
5.3 Central SZ decrement	12
5.4 SZ power spectrum	13
6. Conclusion	15
A. Angle-averaged radial Lorentz force	16

1. Introduction

It has been known that the intracluster medium has magnetic fields of micro-gauss strength. They affect the evolution of galaxies [5], contribute significantly to the total pressure of interstellar gas, are essential for the onset of star formation [59], and control diffusion, confinement and evolution of cosmic rays in the intracluster medium (ICM) [32]. In clusters of galaxies, magnetic fields may play also a critical role in regulating heat conduction (e.g., [11, 42]), and may also govern and trace cluster formation and evolution.

Magnetic fields in the intra-cluster medium have been inferred in various manners using diagnostics such as radio synchrotron relics within clusters, inverse Compton X-ray emissions from clusters, Faraday rotation measures of polarized radio sources within or behind clusters and cluster cold fronts in X-ray ([14, 8]). From these observations it can be inferred that the medium within most clusters is magnetized with typical field strengths at a few μG level distributed throughout the cluster scale. In the cores of "cooling flow clusters" ([21, 64]) and also in cold fronts [65], the field strengths may reach $10\mu\text{G}$ - $40\mu\text{G}$

and could be dynamically important. It is thus essential to study the effect of an intra-cluster magnetic field on the gas density distribution in the ICM.

A very important observational probe of the cluster gas density distribution is the thermal Sunyaev Zeldovich effect [62, 63]. This effect occurs because of the re-scattering of primary CMB photons with the hot electrons in the ICM resulting in secondary anisotropies in the CMB at small angular scales (for a detailed review see [6]). At 30 GHz, anisotropies from the thermal SZ effect are expected to dominate over the primary CMB fluctuations for multipoles $\ell \leq 2500$. The angular power of SZ fluctuation depends sensitively on the integrated cluster abundance and cluster gas distribution (for details see [2]). The SZ effect in clusters depends directly on the density and temperature profile of the ICM. For any particular cluster, it is quantified through the y -parameter which is essentially the temperature decrement along a line of sight through the cluster. This is therefore an important observational probe and can be used to constrain/detect any additional parameter that affects the density of the ICM. In the present work, we study the effect of intracluster magnetic fields on the gas density profile of the ICM and compute the central SZ decrement for different cluster masses as well as the angular power spectrum. To study magnetic field effects in the ICM, earlier authors have incorporated it by introducing the magnetic pressure in the hydrostatic equilibrium condition ([28, 15, 67]). Although this is an important effect, there is, in addition to the pressure, a contribution arising from the tension force due to the field. We show in this paper, that the most general treatment involves using both terms arising out of the Lorentz force due to the field. In general, the detailed form of the magnetic field configuration is unknown and moreover it can vary from cluster to cluster. It is only in the specific case of isotropic configurations, that the magnetic pressure is the only contribution. However, there could be other plausible configurations of magnetic fields in clusters where both the pressure and the tension force contribute. In this paper, we classify the different field configurations and study the problem for a near-radial field.

The paper is organized as follows: Section 2 presents the formulation of the problem by setting up the hydrostatic equilibrium equation incorporating the magnetic field. Sections 3 and 4 present the mathematical formulation of the y -parameter and the CMB angular power spectrum respectively. Section 5 presents the results for the density profiles and SZ observables which are got by solving the hydrostatic equilibrium equation and finally section 6 summarizes the results and concluding remarks.

2. Formulation

In this section, we present the method of incorporating the effect of a generic tangled magnetic field for studying its effect on the ICM gas. We assume that the ICM is in hydrostatic equilibrium in the presence of magnetic field whose effect is incorporated by using the Lorentz force. The typically smooth morphology of the X-ray emission from the hot intra-cluster medium leads naturally to the hypothesis that the gas is in near equilibrium, stratified along isopotential surfaces in a mildly evolving distribution of dark matter, gas and galaxies. This suggests that the assumption of hydrostatic equilibrium for such relaxed clusters is mostly justified. The dark matter mass profile and the temperature

profile are specified by their ‘universal’ forms as described in the following sections. The radial profile of the magnetic field is also implicitly specified by its dependence on the density profile. Given these profiles, the gas density is finally solved perturbatively around the default profile (i.e the profile in the absence of magnetic field). The perturbation method is only applicable for small magnetic field values (in this case, it can be used for values of the central field upto $\sim 4\mu\text{G}$).

2.1 Dark matter density profile

The gravitational potential within clusters is mainly determined by dark matter. The dark matter density profile, $\rho_{\text{dm}}(r)$ suggested by many high resolution N - body simulations is well described by the NFW profile ([43, 44])

$$\rho_{\text{dm}} = \rho_s y_{\text{dm}}(x) = \rho_s \frac{1}{x(1+x)^2} \quad (2.1)$$

Here, $x = r/r_s$ is the radius in unit of core radius r_s and ρ_s is a normalization factor which represents the characteristic density at $r = r_s$. Since the dark matter density profile is self-similar, the dark matter mass profile is also self-similar. So, the dark matter mass enclosed within a radius r is

$$M(\leq r) = 4\pi\rho_s r_s^3 m(r/r_s) \quad (2.2)$$

where, $m(x)$ is a non-dimensional mass profile given by

$$m(x) = \int_0^x du u^2 y_{\text{dm}}(u) = \ln(1+x) - \frac{x}{(1+x)}; \quad (2.3)$$

The definition of the virial radius, R_{vir} , is the radius within which the total dark matter mass is confined, i.e., $M_{\text{vir}} \equiv M(\leq c)$, where

$$c \equiv \frac{R_{\text{vir}}}{r_s} \quad (2.4)$$

is a dimensionless parameter called the ‘concentration parameter’. Evaluating equation (2.2) at the virial radius, the normalization factor, ρ_s , is fixed at;

$$\rho_s = c^3 \frac{M_{\text{vir}}}{4\pi R_{\text{vir}}^3 m(c)} \quad (2.5)$$

The virial radius, $R_{\text{vir}}(M_{\text{vir}}, z)$ is calculated with the spherical collapse model [45],

$$R_{\text{vir}} = \left[\frac{M_{\text{vir}}}{(4\pi/3)\Delta_c(z)\rho_c(z)} \right]^{1/3} = \left[\frac{M_{\text{vir}}c^3}{4\pi\rho_s m(c)} \right]^{1/3} \quad (2.6)$$

where the second equality comes from evaluating R_{vir} from equation (2.5). Here $\Delta_c(z)$ is the spherical over-density of the virialized halo within R_{vir} at z , in units of the critical density of the universe at z , $\rho_c(z)$. Following [29], we assume a value $\Delta_c(z=0) = 100$ for a cosmological model with $\Omega_m = 0.29$ and $\Omega_\Lambda = 0.71$.

We follow [7] in adopting the approximation for c as a function of the virial mass of the cluster. They give the median values of ‘ c ’ and also the 1σ deviations:

$$c = K \left(\frac{M_{\text{vir}}}{1.5 \times 10^{13} h^{-1} M_{\odot}} \right)^{-0.13} \quad (2.7)$$

with $K = 9$ reproducing the best-fit and $K = 13.5$ and $K = 5.8$ reproducing the $+1\sigma$ and the -1σ values in the concentration parameter. These values of the concentration parameter are also consistent with the findings of [60].

The above set of equations specify the dark matter density profile of a particular mass cluster.

2.2 Universal temperature profile

The “universal temperature profile” used for our calculation [34] is (normalized by the emission-weighted temperature):

$$\frac{T}{\langle T \rangle} = \frac{T_0}{\left(1 + \frac{r}{a_x}\right)^{\delta}} \quad (2.8)$$

where $\langle T \rangle$ is the emission-weighted temperature of the cluster, $T_0 = 1.33$, $a_x = R_{\text{vir}}/1.5$, and $\delta = 1.6$ on the radial range $(0.04-1.0) R_{\text{vir}}$. To determine the emission-weighted temperature from the cluster mass, we use a relation that arises from adiabatic evolution of the gas in cluster. [1] have shown that the observations of [23] of $M_{500}-\langle T \rangle$ relation in clusters can be understood from gravitational processes alone. We therefore use this empirical relation ($M_{500}-\langle T \rangle$) derived by [24]:

$$M_{500} = (2.64_{-0.34}^{+0.39}) 10^{13} M_{\odot} \left(\frac{k_b \langle T \rangle}{1 \text{ keV}} \right)^{1.78_{-0.09}^{+0.10}} \quad (2.9)$$

where k_b is the Boltzmann constant and M_{500} has been calculated self-consistently by taking the total mass within the radius where the over-density is $\delta \geq 500$.

2.3 Hydrostatic equilibrium of gas in presence of magnetic field

In this section, we determine the density profile of the gas in the ICM given the universal temperature profile and assuming that the gas is in hydrostatic equilibrium (HE) with the background dark matter in the presence of a tangled magnetic field specified by a profile $B(r)$.

2.3.1 Density profile in the absence of magnetic field

The HE equation for the gas in the absence of a magnetic field has the well-known form:

$$\frac{1}{\rho_g(r)} \frac{dP_g(r)}{dr} = -\frac{GM(\leq r)}{r^2} \quad (2.10)$$

where G is the gravitational constant, $\rho_g(r)$ and $P_g(r)$ are the density and pressure profiles respectively. The pressure is related to the density through the equation of state:

$$P(r) = \frac{\rho(r) k_B T(r)}{\mu m_p} \quad (2.11)$$

Here, $M(\leq r)$ is the mass enclosed within radius r and μ and m_p denote the mean molecular weight ($\mu = 0.59$) and the proton mass. $T(r)$ is the universal temperature profile of the gas. $M(\leq r)$ is mainly determined by the dark matter mass profile. The solution $\rho_g(r)$ to the above HE equation is referred to as the default density profile. Using the equation of state, the HE equation can be recast as:

$$\frac{k_B}{\mu m_p} \left(\frac{d \ln \rho_g}{dr} + \frac{d \ln T(r)}{dr} \right) = - \frac{GM(\leq r)}{r^2 T(r)} \quad (2.12)$$

The solution $\rho_g(r)$ to the above can then be expressed as :

$$\frac{\rho_g(r)}{\rho_g(0)} = \frac{T(0)}{T(r)} \exp \left(- \frac{\mu m_p}{k_B} \int_0^r dr \frac{GM(\leq r)}{r^2 T(r)} \right) \quad (2.13)$$

The central density $\rho_g(0)$ is fixed by the constraint that the gas mass within the cluster is a 'universal' fraction of the total mass of the cluster. Thus, the gas fraction $f_{\text{gas}} = M_{\text{gas}}/M_{\text{total}}$ within the virial radius is taken to be universal and equal to 0.105, as recently found by Ettori (2003) for a sample of low and high redshift clusters. The gas mass can be expressed as:

$$M_{\text{gas}} = 4\pi \int_0^{r_{\text{vir}}} dr r^2 \rho_g(r) \quad (2.14)$$

Since the total gas mass is negligible compared to the dark matter, $M_{\text{total}} \approx M_{\text{dm}}$, mass in dark matter, and therefore $f_{\text{gas}} \approx M_{\text{gas}}/M_{\text{dm}}$.

2.3.2 Density profile in the presence of magnetic field

The effect of magnetic fields is now taken into account by introducing an additional term corresponding to the radial component of the Lorentz force due to the field. The Lorentz force due to a tangled magnetic field $\vec{B}(\vec{r})$ is given by

$$\vec{F}(\vec{r}) = \vec{B}(\vec{r}) \times (\nabla \times \vec{B}(\vec{r})) \quad (2.15)$$

The Lorentz force depends on the magnetic field configuration which is not known and moreover its detailed form could vary from cluster to cluster. However since we are looking at only the radial profiles, we incorporate the effect of magnetic field by considering the angle-averaged radial Lorentz force $\langle F_r \rangle$. We then simplify the angle-averaged Lorentz force by explicitly writing it down in terms of the angular averages of the field components (i.e in terms of $\langle B_r^2 \rangle, \langle B_\theta^2 \rangle, \langle B_\phi^2 \rangle$). This method has been used in the context of studying magnetic field effects on the spherical collapse of non-rotating low-mass gas clouds [12] and also in the context of spherical accretion onto a black-hole in the presence of magnetic field [58].

It is important to note here, that the Lorentz force due to magnetic field consists of two terms, one term which is a pure gradient $\vec{\nabla} B^2$, known as magnetic pressure and the other one being $(\vec{B} \cdot \vec{\nabla}) \vec{B}$ known as magnetic tension. Although these two terms contain the gradient operator $\vec{\nabla}$, they are not identical. The magnetic pressure is a pure gradient $\partial B^2 / \partial r$, and hence is directly tied to the gradient of the underlying gas density distribution. So for instance, if the gas density profile is nearly flat, then magnetic pressure has a negligible contribution. On the other hand, the magnetic tension is not a pure gradient.

The magnetic tension component along the radial direction can be written as: $(\vec{B} \cdot \vec{\nabla})B_r = \vec{\nabla} \cdot (\vec{B}B_r)$, (using the fact that $\vec{\nabla} \cdot \vec{B} = 0$). Hence this tension component is a divergence and hence consists of two sub-terms, one of which is like $\partial B^2 / \partial r$ (pressure-like term) and the other is like B^2 / r . This non-pressure like term also known as "hoop stress" acts opposite to the pressure gradient and increases towards the center. Refer to Eq A11 and A12. We use eq A12 for the derivation of density profiles. We have also included the very special single case of equal field components also for reference. It is only in this case that the Lorentz force has a pressure-like term. But in our work we consider generic cases in which the hoop stress contributes.

We classify the different sets of field configurations in terms of the relative strengths of the radial and transverse correlations (For details refer to the Appendix). Previous studies have mainly focused on the isotropic configuration in which the relative strengths of the three correlations are equal. In this case it can be shown, that the angle- averaged Lorentz force acts like a magnetic pressure. However this is only a special configuration. We consider a generic set of configurations in which the radial component of the magnetic field is auto-correlated, while the correlation between the transverse(polar) components is negligibly small.

To begin with, the HE equation in the presence of tangled magnetic fields has the form:

$$\frac{1}{\rho_B(r)} \frac{dP_B(r)}{dr} = -\frac{GM(\leq r)}{r^2} + \langle F_r \rangle \quad (2.16)$$

In this case too, the equation of state is specified by

$$P_B = \frac{\rho_B(r)k_b T_B(r)}{\mu m_p} \quad (2.17)$$

where $\rho_B(r)$, $P_B(r)$ and $T_B(r)$ are the modified density, pressure and temperature profiles respectively in the presence of the magnetic field.

In order to attempt to solve the equation for the modified density profile $\rho_B(r)$ we make some simplifications. Firstly we assume that the field-strength is not very large so that a perturbative solution around the default density profile $\rho_g(r)$ can be attempted. For this to be true, the energy density in the magnetic field should be small compared to the gravitational energy density corresponding to the default gas density. The next thing to note is that the change in the default temperature profile will be negligible (i.e $T_B(r) = T_g(r)$) since we do not consider any additional energy transfer to the gas from the magnetic field. We use the universal temperature profile as an input to deduce the density profile since its a good fit to observations. Since we use a perturbative scheme, the change in the temperature profile due to magnetic field contributes at only higher order in perturbation theory and hence can be neglected. Under these assumptions we can combine the two equations (2.10) and (2.16) to get:

$$\rho_B(r) = \rho_g(r) \left(1 + \frac{\mu m_p}{k_B} \int_r^a dr \frac{\langle F_r \rangle(r)}{\rho_g(r)T(r)} \right) \quad (2.18)$$

In this case, the gas fraction $f_{\text{gas}} = M_{\text{gas}}/M_{\text{total}}$ is considered to be ‘universal’ too and equal to 0.105. The upper limit a in the above integral is determined from the relation:

$$M_{\text{gas}} = 4\pi \int_0^{r_{\text{vir}}} dr r^2 \rho_{\text{B}}(r) \quad (2.19)$$

In order to compute the modified profile $\rho_{\text{B}}(r)$, it remains to specify the radial profile of the angle-averaged Lorentz force $\langle F_{\text{r}}(r) \rangle$. As shown in the Appendix, $\langle F_{\text{r}} \rangle$, in turn, can be expressed in terms of the angle-averages of the squared magnetic field components viz. $\langle B_{\text{r}}^2 \rangle$, $\langle B_{\theta}^2 \rangle$ and $\langle B_{\phi}^2 \rangle$. Thus the form for $F_{\text{r}}(r)$ depends on the relation between the different component profiles.

In the present work, we compute the results for field configurations which are nearly radial. i.e $B^2 = B_{\text{r}}^2$. For such configurations, the form for $F_{\text{r}}(r)$ is given in eq(A12). It thus remains to specify only the field strength profile $B(r)$ and this is done below. The magnetic field profile is assumed to be of a parametric form,

$$B(r) = B_* \left(\frac{\rho_{\text{g}}(r)}{\rho_{\text{g}}(z=0)} \right)^{\alpha} \quad (2.20)$$

Here, $\rho_{\text{g}}(z=0)$ is the average cosmological density of the gas at $z=0$, B_* is measured in μG and α is a parameter $\geq 2/3$. The above form is suggested by the rotation measure (RM)-X-ray correlation inferred in simulations/observations. (see, e.g., [8, 20]). In this paper, we assume the value $\alpha = 0.9$ for our calculations.([20]).

3. Compton y -parameter and central SZ decrement

The temperature decrement of CMB due to the SZ effect is directly proportional to the Compton parameter (y). For a spherically symmetric cluster, the Compton parameter is given by

$$y = 2 \frac{\sigma_{\text{T}}}{m_{\text{e}} c^2} \int_0^R p_{\text{e}}(r) dl \quad (3.1)$$

where σ_{T} is the Thomson cross-section, and $p_{\text{e}}(r) = n_{\text{e}}(r) k_{\text{b}} T_{\text{e}}(r)$ is the electron pressure of the ICM, where $n_{\text{e}}(r) = 0.875(\rho_{\text{gas}}/m_{\text{p}})$ is the electron number density, k_{b} is the Boltzmann constant, and $T_{\text{e}}(r)$ is the electron temperature. The integral is performed along the line-of-sight (l) through the cluster and the upper limit of the integral ($+R$) is the extent of the cluster along any particular line-of-sight. We do not include the effects of beam size in calculating the y parameter. This approximation is justified by the fact that the pressure profiles are relatively flat in the inner region. The variation of pressure integrated along the line-of-sight as a function of the projected radius is even flatter thus providing more justification for the above approximation.

The angular temperature profile projected on the sky due to SZ effect, $\Delta T(\theta)/T_{\text{CMB}}$ is given in terms of the Compton parameter in equation (3.1)

$$\frac{\Delta T(\theta)}{T_{\text{CMB}}} = g(x)y(\theta), \quad (3.2)$$

where $g(x) \equiv x \coth(x/2) - 4$, $x \equiv h\nu/k_B T_{\text{CMB}}$, $T_{\text{CMB}} = 2.728$ [25]. In the Rayleigh-Jeans approximation, $g(x) \approx -2$. We only evaluate “central” SZ decrement from the pressure profiles of our models. In this case, the integral in equation (3.1) reduces to

$$y_0 = 2 \frac{\sigma_T}{m_e c^2} \int_0^R p_e(r) dr \quad (3.3)$$

In the Rayleigh-Jeans part of the CMB spectrum, the deviation from the black-body spectrum results in a decrement of the CMB temperature,

$$\Delta T_{\mu w 0} \approx -5.5 y K \quad (3.4)$$

We use the pressure profiles resulting from our model to calculate the central SZ decrement in the temperature of the CMB.

4. Angular power spectrum

The angular two-point correlation function of the SZ temperature distribution in the sky is conventionally expanded into the Legendre polynomials:

$$\left\langle \frac{\Delta T}{T_{\text{CMB}}}(\hat{\mathbf{n}}) \frac{\Delta T}{T_{\text{CMB}}}(\hat{\mathbf{n}} + \theta) \right\rangle = \frac{1}{4\pi} \sum_{\ell} (2\ell + 1) C_{\ell} P_{\ell}(\cos \theta) \quad (4.1)$$

Since we consider discrete sources, we can write $C_{\ell} = C_{\ell}^{(P)} + C_{\ell}^{(C)}$, where $C_{\ell}^{(P)}$ is the contribution from the Poisson noise and $C_{\ell}^{(C)}$ is the correlation among clusters ([45], § 41). We define the frequency independent part in the power spectrum as $C_{\ell}^{*(P)} \equiv C_{\ell}/g^2(x)$. The integral expression of $C_{\ell}^{*(P)}$ can be derived following [16] as

$$C_{\ell}^{*(P)} = \int_0^{z_{\text{dec}}} dz \frac{dV}{dz} \int_{M_{\text{min}}}^{M_{\text{max}}} dM \frac{dn(M, z)}{dM} |y_{\ell}(M, z)|^2, \quad (4.2)$$

where $V(z)$ is the co-moving volume and y_{ℓ} is the angular Fourier transform of $y(\theta)$ given by

$$y_{\ell} = 2\pi \int y(\theta) J_0[(\ell + 1/2)\theta] \theta d\theta, \quad (4.3)$$

where J_0 is the Bessel function of the first kind of the integral order 0. In equation (4.2), z_{dec} is the redshift of photon decoupling and dn/dM is the mass function of clusters which is computed in the Press-Schechter formalism [51]. The mass function has been computed using the power spectrum for a Λ -CDM model with normalization of $\sigma_8 = 0.8$. We choose $M_{\text{min}} = 5 \times 10^{13} M_{\odot}$ and $M_{\text{max}} = 2 \times 10^{15} M_{\odot}$ and integrate till redshift of $z = 5$ instead of z_{dec} . This is done because the integral in equation (4.2) is found to be insensitive to the upper limit in redshift beyond $z = 4$, the reason being that the mass function is exponentially suppressed beyond that redshift in this mass range

5. Results & Discussion

In this section, we investigate the effects of the magnetic field with nearly radial configuration on the density profiles, the central SZ decrement and on the SZ angular power spectrum. We also present a discussion on the other possible configurations of the cluster magnetic field and the Lorentz force arising out of these configurations.

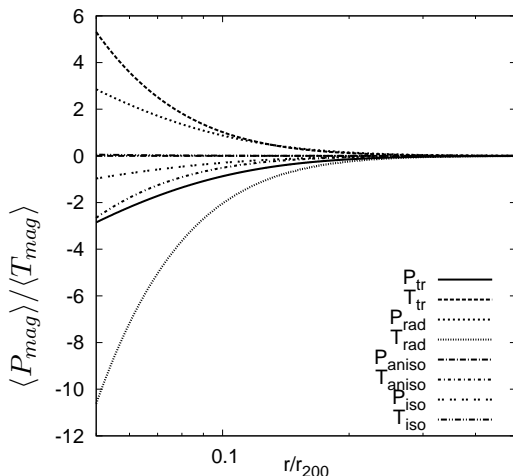


Figure 1: Pressure (P_{mag}) and tension (T_{mag}) forces arising out of the magnetic Lorentz force as a function of the scaled distance for different magnetic field configurations like transverse (tr), isotropic (iso), anisotropic (aniso) and nearly radial (rad). The pressure and tension terms are computed with arbitrary normalization

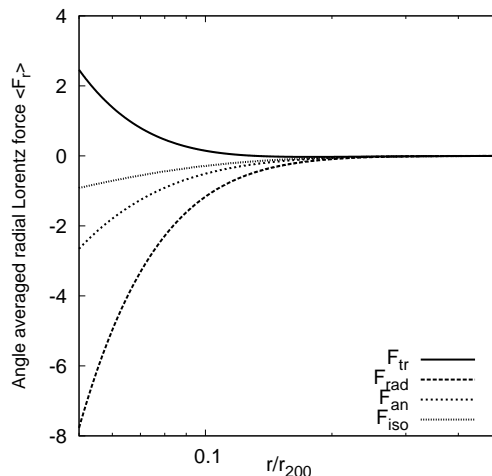


Figure 2: Angle averaged Lorentz force calculated for different magnetic field configurations. All the numerical factors have been normalized to unity

5.1 Magnetic field configurations and Lorentz force

The Lorentz force can be split into two terms : the magnetic pressure ($\propto d(B^2)/dr$) which depends on the gradient of the field strength and the magnetic tension ($\propto B^2/r$) which depends on the field strength (as shown in detail in the Appendix). In figure (1), we plot the radial dependence of the magnetic pressure and the magnetic tension for different field configurations viz. radial ($\langle B_T^2 \rangle = 0$), transverse ($\langle B_r^2 \rangle = 0$), anisotropic ($\langle B_T^2 \rangle = 0.5\langle B^2 \rangle$) and isotropic ($\langle B_r^2 \rangle = \langle B_\theta^2 \rangle = \langle B_\phi^2 \rangle = 0.33\langle B^2 \rangle$). In figure (2), we plot the resultant Lorentz force (sum of pressure and tension) for the same set of configurations. To demonstrate the behaviour of magnetic pressure and tension forces as well as the angle-averaged radial Lorentz force as a function of scaled radius of the cluster, we have normalized all the constants to unity in both the figures. We also use the convention that positive values correspond to force directed radially outwards whereas negative values correspond to force directed radially inwards while plotting. As seen in figure (1), for the

radial configuration, the tension force dominates over the pressure force and the net force is directed radially inwards as we approach the central region ($r \leq 0.2r_{200}$) of the cluster. This causes an enhancement in the gas density relative to the default state. This is different to the manner in which the effect of the magnetic Lorentz force is usually incorporated in the hydrostatic equilibrium equation for the cluster gas.

For the *transverse* configuration, the tension force dominates over pressure force and is directed outwards as a result of which, the net force is directed outwards as we approach the central region. This will possibly cause a decrement in the gas density relative to the default case. In such models, the magnetic field can act as a heating source in the ICM.

In the *anisotropic* case, the pressure force vanishes whereas the tension force is directed inwards and thus the net force is directed inwards. In the *isotropic* configuration, the tension force vanishes whereas the pressure force is directed inwards and thus the net force is directed inwards. In both these cases, the gas tends to fall towards the central region thus causing an enhancement in gas density relative to the default scenario.

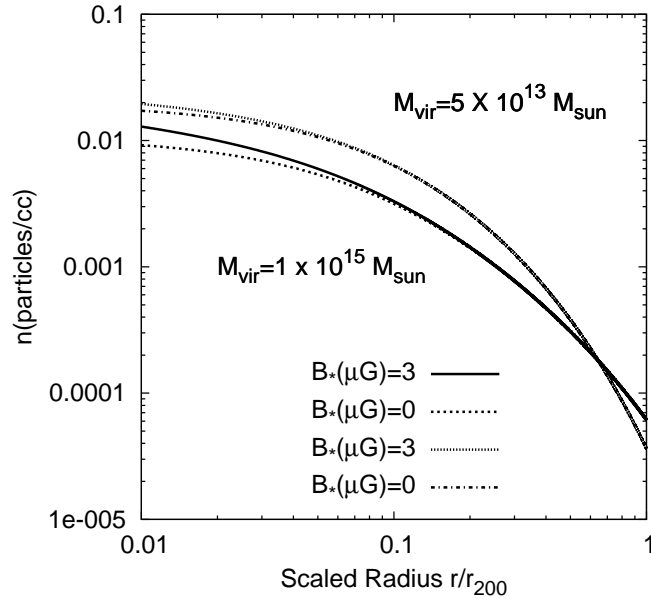


Figure 3: Density versus scaled radius r/r_{200} for cluster masses $5 \times 10^{13}M_{\odot}$ and $1 \times 10^{15}M_{\odot}$

5.2 Density profiles

Using the NFW profile for dark matter and the ‘universal’ temperature profile, the hydrostatic equilibrium equation is solved to get the density profiles for different magnetic field strengths for a given cluster mass. We consider the range of cluster masses $5 \times 10^{13} - 1 \times 10^{15}M_{\odot}$.

In figure (3), the density profile (in units of particles/cc) is plotted as a function of the scaled radius r/r_{200} for a clusters of mass $5 \times 10^{13}M_{\odot}$ and $1 \times 10^{15}M_{\odot}$ for different values of field strengths specified by B_* . As seen in figure (3), the presence of magnetic

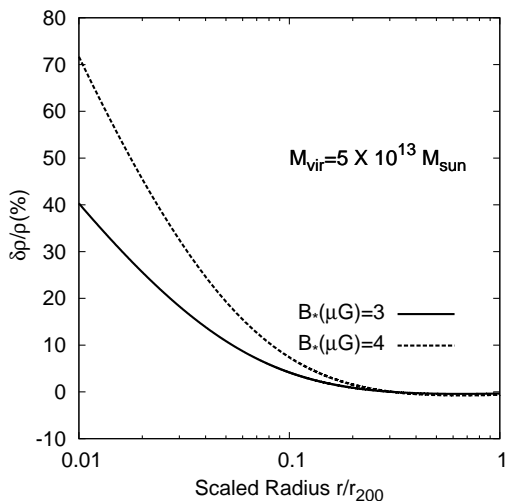


Figure 4: Fractional change in density due to magnetic fields of strength $3 \mu\text{G}$ and $4 \mu\text{G}$ versus scaled radius r/r_{200} for a cluster mass $5 \times 10^{13} M_{\odot}$

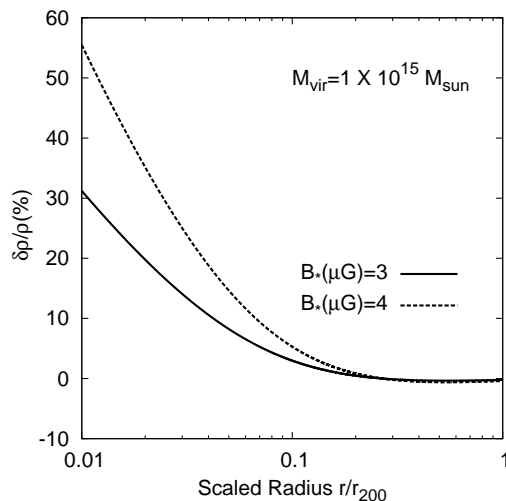


Figure 5: Fractional change in density due to magnetic fields of strength $3 \mu\text{G}$ and $4 \mu\text{G}$ versus scaled radius r/r_{200} for a cluster mass $1 \times 10^{15} M_{\odot}$

field causes an enhancement in the gas density compared to the default (i.e no magnetic field) value for a particular cluster. The enhancement is large in the central regions and decreases outwards. There is a crossover from enhancement to depletion which occurs at $r_{\text{cro}} = 0.2r_{200}$. At distances greater than the crossover radius there is a depletion in the gas density. This occurs because of the fact that the Lorentz force contributes through two opposing forces viz. the magnetic tension and magnetic pressure. The magnetic tension dominates in the central regions whereas magnetic pressure dominates in the outer regions. The magnetic tension acts inward and hence pushes the gas inwards increasing the density whereas in the outer regions (where magnetic pressure dominates) the magnetic force acts outward and pushes the gas outwards, depleting the density.

In figures 4 and 5, the fractional percentage density change is plotted for masses $5 \times 10^{13} M_{\odot}$ and $1 \times 10^{15} M_{\odot}$ respectively. There is nearly a 70% increase in the density towards the central region of the cluster of mass $5 \times 10^{13} M_{\odot}$ for a magnetic field strength of $4 \mu\text{G}$. For a higher cluster mass this fractional change in density is lower as seen in Figure 3. The extent of density enhancement for a given magnetic field strength thus shows a trend with cluster mass, the enhancement decreasing with increasing mass. In other words, the effect of a magnetic field of given strength on the gas density is higher for low-mass clusters and groups.

This enhancement of density in the central regions has important implications for the Sunyaev Zeldovich effect since the temperature decrement for an individual cluster depends directly on the gas density. This in turn also gets reflected in the CMB angular spectrum on small scales or high multipoles. We discuss these issues in the following sections.

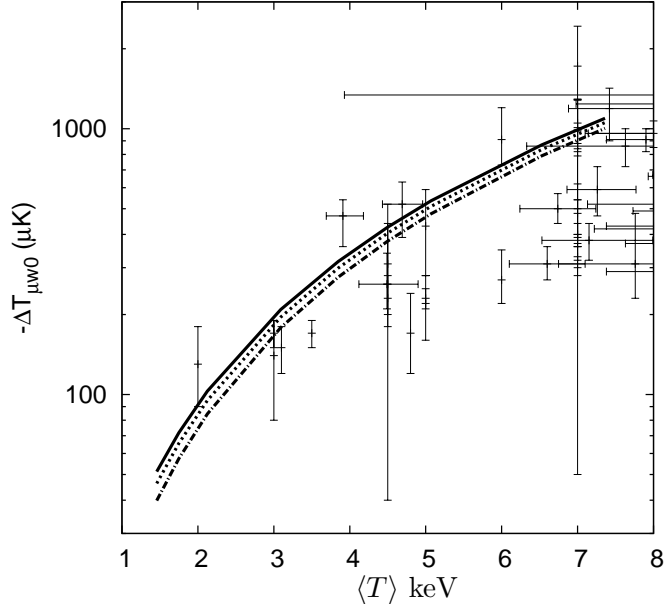


Figure 6: Observed and predicted relations of central SZ decrement ($\Delta T_{\mu w 0}$ (μK)) versus emission-weighted temperature ($\langle T \rangle$ (keV)) in clusters. The solid line corresponds to magnetic field strength $B_* = 4\mu\text{G}$, the dotted line corresponds to $B_* = 3\mu\text{G}$ and the dot-dashed line corresponds to $B_* = 0\mu\text{G}$. Data points have been taken from Zhang & Wu 2000, McCarthy et al. 2003 and references therein and Lieu, Mattiz, & Zhang 2006

5.3 Central SZ decrement

Using the density profiles, the pressure profiles are evaluated and the resulting central SZ decrement is computed as a function of the cluster mass. In figure (6), the central SZ decrement is plotted as a function of the emission-weighted temperatures of the cluster. For comparison, we have also plotted the data for the central SZ decrement for a sample of clusters taken from [68, 39] and references therein and observed with WMAP [33].

From figure (6), it can be seen that the temperature decrement is enhanced in the presence of magnetic fields and increases with the emission weighted temperature (and hence the cluster mass). The effect of the magnetic field is more pronounced for low mass clusters. In particular, magnetic fields of strength $\sim 3\mu\text{G}$ cause nearly a 25 % increase in the SZ decrement for a cluster with emission weighted temperature ~ 2 keV corresponding to a virial mass of $1 \times 10^{14} M_\odot$. Thus from precise SZ observations of low mass clusters and galaxy groups it might be possible to detect or place constraints on the field strength in these structures.

Currently proposed SZ experiments are expected to make wide angle surveys of the CMB sky with a resolving power of upto few arc minutes. Experiments such as South Pole Telescope (SPT) and Atacama Cosmology Telescope (ACT) can survey several hundreds of square degrees upto a mass limit $2 \times 10^{14} M_\odot$ with high sensitivity at arc minute resolution [56]. In particular, the SPT survey will cover 4000 deg^2 of sky with $10\mu\text{K}$ sensitivity per 1 arc minute pixel at 150 GHz and is expected to yield nearly 10000 clusters with masses

greater than $2 \times 10^{14} M_{\odot}$ [9]. The ACT survey is expected to map 200 square degrees of CMB sky in 3 frequency bands of 145 GHz, 220 GHz and 265 GHz at arc minute resolution reaching sensitivity levels of $2 \mu\text{K}$ per pixel [37]. However to detect the CMB temperature decrement in the central regions it is necessary to be able to resolve features at the level of a few arc seconds. This is because the cluster virial radius (~ 1 Mpc) corresponds to angular scale of arc minutes whereas the central regions (~ 100 kpc) will typically correspond to an angular scale of few arc seconds. There are upcoming proposals which will probe such scales. In particular, the Cornell-Caltech Atacama Telescope (CCAT) [26] is proposed to do high angular resolution follow-up observations of clusters which have already been detected in some of the above mentioned wide-area surveys. The 150 GHz camera on CCAT would be sensitive at $310 \mu\text{K s}^{1/2}$ with an angular resolution of nearly 3 arc seconds per pixel. These experiments will thus provide a statistically large sample of clusters using which it would be possible to detect or put proper constraints on the ICM magnetic field strengths.

5.4 SZ power spectrum

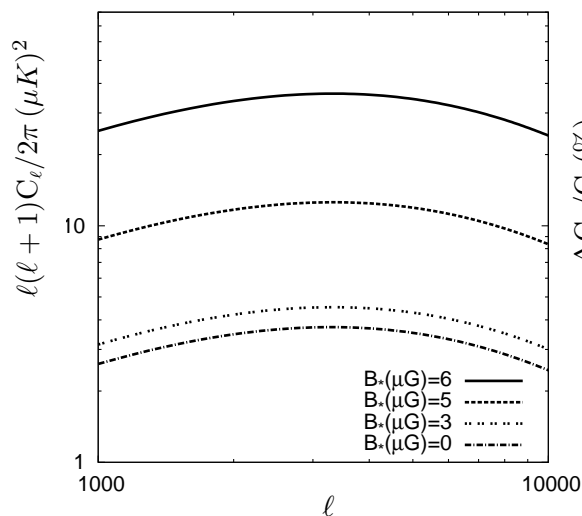


Figure 7: Poisson contribution to the angular power spectrum of the SZ fluctuations plotted as a function of ℓ

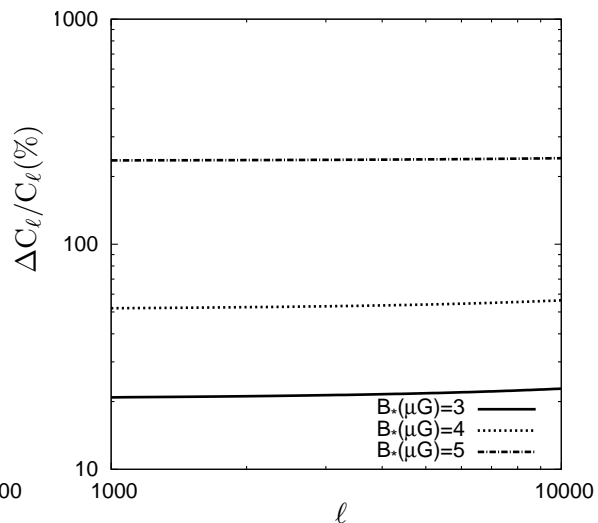


Figure 8: Fractional change in angular SZ power for different magnetic field strengths plotted as a function of ℓ

The results for the SZ angular power spectrum are presented in figure (7). The power spectra are plotted for different magnetic field strengths and the power spectra for the default density and temperature profiles is also plotted for comparison. It can be seen that the power peaks close to $\ell = 3300$ for a field strength of $3 \mu\text{G}$ and the peak shifts to higher ℓ values as the field strength increases. This means strong magnetic fields have a dominant effect on small scales. The typical value of the SZ power for a field strength of $3 \mu\text{G}$ is $3.2 \mu\text{K}^2$. The SZ power increases with increasing magnetic field strength. In the figure, we have plotted the results for magnetic field strengths upto $6 \mu\text{G}$. The perturbative estimate is applicable only for field strengths upto $3 \mu\text{G}$. The SZ power increases with increasing

magnetic field strength as can be seen in the figure. We can extrapolate this trend to estimate the CMB power at larger values of field strengths (\sim the order of few-tens of micro-Gauss, as has been observed in clusters) by a simple qualitative scaling argument. Since the magnetic field depends on density as $B \propto \rho^{2/3}$, and the y-parameter (which is the fractional temperature change) is directly proportional to density $\Delta T/T \propto \rho$, we deduce that the CMB angular power which scales as temperature squared will scale with magnetic field as $C_\ell \propto B^3$. From this we can see that for magnetic fields of strength $\sim 15\text{-}20\mu\text{G}$, the CMB power will increase by a factor of nearly 125-300 times compared to the power estimated for $3\mu\text{G}$. This means that the linearly extrapolated estimate of CMB power for a $15\mu\text{G}$ field will be $\sim 400\mu\text{K}^2$. In figure (7), C_ℓ for field strengths $5\mu\text{G}$ and $6\mu\text{G}$ are plotted using this scaling estimate.

In figure (7), we have plotted the percentage change in the angular power of CMB compared to the default case. It can be seen from the figure that a $3\mu\text{G}$ field induces a 20% increase in the CMB power whereas a $4\mu\text{G}$ induces a 40 % change.

Observations by CBI [52] and BIMA [18] report an excess in CMB anisotropy at $\ell \geq 2000$. The primary anisotropies at these scales are damped out and the cause of this excess is attributed to the SZ power spectrum from galaxy clusters. CBI 5 year data collected at 30 GHz [61] report the level of anisotropies at $\ell \sim 3000$ to be $380\mu\text{K}^2$ with a Gaussian error of $117\mu\text{K}^2$. An excess at nearly 1σ level is also reported by the ACBAR experiment [54] at 150 GHz at these scales. Attributing this excess to the SZ effect alone (without the inclusion of magnetic fields) would require the normalization of matter power spectrum $\sigma_8 \sim 1$. WMAP 5 year results [30] however have ruled out this value and fixed $\sigma_8 \sim 0.8$. As a result, this excess cannot be explained by the ordinary SZ effect alone and additional possible effects which might contribute have to be investigated (see for e.g [35]). However as we discussed above, if magnetic fields are present generically at the level of tens of μG , then it might be possible to reconcile with this $\sigma_8 \sim 0.8$.

Recent observations conducted by the Sunyaev Zeldovich Array (Sharp et al. 2009) do not report any excess and estimate the constraint on the level of secondary anisotropies to be $14_{-62}^{+71}\mu\text{K}^2$. APEX-SZ has measured the CMB angular power at a frequency of 150 GHz in the range of $3000 \leq \ell \leq 10000$ and report anisotropies at the level $33_{-24}^{+37}\mu\text{K}^2$ at effective $\ell \sim 5000$ [53]. These experiments detect much less power compared to CBI, BIMA etc. The CMB anisotropy power at this value would then limit the generic magnetic field strength to $\sim 7 - 8\mu\text{G}$. Several upcoming CMB experiments, such as the Atacama Cosmology Telescope (ACT), Planck etc claim to reach upto the cosmic variance limit and measure the SZ power to an accuracy of nearly 1 % (see the science white paper [41]).

The central SZ decrement and the angular power spectrum depend strongly on the magnetic field configuration as well. In this work we have explored the effects of a nearly radial magnetic field. However, there could be other possibilities in which the effects could be different and might even be opposite to our calculations. The extreme case where the tension force goes to zero and we are left with only the pressure term is the isotropic configuration which has been addressed in earlier works by several authors [15, 28]. Here there is a suppression in the central SZ decrement and thus in the angular power, since the magnetic field will act as a heating source and push the gas out of the central regions. In the

other two cases, the effect of the magnetic field on central SZ decrement and angular power will vary according to the geometry of the field (as explained in the the figures (1) and 2. Thus this can be possibly used as an indirect probe of the magnetic field configurations in the intracluster medium.

Thus it is extremely important to model the effects of intracluster magnetic fields in addition to the standard effects in order to calculate the SZ power spectrum much more precisely for different field configurations.

6. Conclusion

In this work, we have studied the effect of an intracluster tangled magnetic field on the gas distribution in the ICM. In addition, we have also investigated the effect of cluster magnetic fields on the central SZ decrement for a range of cluster masses. We have also computed the CMBR angular spectrum for different field strengths . In contrast to previous studies, we incorporated the complete radial Lorentz force due to the magnetic field in the hydrostatic equilibrium equations, thereby introducing the effect of magnetic tension as well in addition to magnetic pressure for a generic field configuration. It is only in the special case of an isotropic configuration that magnetic pressure is the sole contribution. However, realistic cases would involve a range of configurations. In particular we presented the results for a nearly radial magnetic field configuration. The results would be more pronounced for a configuration of magnetic fields in which the tension force is dominant.

It would be interesting to look at all the other important baryonic effects present in the cluster gas like AGN heating, cosmic-ray heating and the like in addition to this effect of the magnetic field to determine the structure of the intracluster gas in more detail and to disentangle various contributions.

Our results can thus be summarized as follows:

1. For a nearly radial magnetic field, the ICM gas density shows an enhancement in the regions close to the center whereas there is depletion in the outer regions, the crossover scale being dependent on the cluster mass.
2. The gas density enhancement/depletion is large for low-mass clusters.
3. The central SZ decrement is enhanced compared to the default (i.e no magnetic field) case if magnetic field effects are included because of the enhancement in the gas density
4. The CMB angular power is also enhanced in the presence of magnetic fields and future precise observations on these small scales can be used to constrain the strength of such fields and their configurations.
5. For an isotropic field configuration, the effects can be opposite to what we have concluded in this piece of work, as pointed out by earlier authors.

Acknowledgments

We thank Dr. Shiv Sethi, Dr. Biman Nath and Dr. Subhabhrata Majumdar for discussions and suggestions.

A. Angle-averaged radial Lorentz force

The Lorentz force due to a magnetic field \vec{B} is given by

$$\vec{F} = \frac{\vec{B} \times (\nabla \times \vec{B})}{4\pi} \quad (\text{A.1})$$

This can also be written as :

$$4\pi\vec{F} = \frac{1}{2}\nabla(B^2) - (\vec{B} \cdot \nabla)\vec{B} \quad (\text{A.2})$$

In spherical polar coordinates, the Lorentz force can be written in terms of its components as $\vec{F} = \hat{r}F_r + \hat{\theta}F_\theta + \hat{\phi}F_\phi$. In particular, the radial component of the Lorentz force F_r can be expressed as:

$$4\pi F_r = \frac{B_\phi}{r \sin \theta} \frac{\partial B_r}{\partial \phi} - \frac{B_\phi}{r} \frac{\partial}{\partial r} (r B_\phi) - \frac{B_\theta}{r} \frac{\partial}{\partial r} (r B_\theta) + \frac{B_\theta}{r} \frac{\partial B_r}{\partial \theta} \quad (\text{A.3})$$

Adding $B_r(\nabla \cdot \vec{B})$ to the R.H.S this can be further rewritten as:

$$4\pi F_r = \nabla \cdot (B_r \vec{B}) - \frac{B_r^2}{r} - \frac{1}{2} \frac{\partial}{\partial r} (B^2) \quad (\text{A.4})$$

Here, $B_r^2 = B_\phi^2 + B_\theta^2$, denotes the transverse part of the expression. We now evaluate the angular average of F_r . The angle averaged Lorentz force is defined as:

$$\langle F_r \rangle = \int \frac{d\Omega}{4\pi} F_r \quad (\text{A.5})$$

Taking the angular average of Eq (A.4), we get:

$$4\pi \langle F_r \rangle = \langle \nabla \cdot (B_r \vec{B}) \rangle - \frac{\langle B_r^2 \rangle}{r} - \frac{1}{2} \frac{\partial}{\partial r} (\langle B^2 \rangle) \quad (\text{A.6})$$

To get a simplified expression for the above angular average, the angle average $\langle \nabla \cdot (\vec{B} B_r) \rangle$ remains to be evaluated. This can be done in the following manner. Let

$$f(r) = \langle \nabla \cdot (\vec{B} B_r) \rangle = \int \frac{d\Omega}{4\pi} \nabla \cdot (\vec{B} B_r) \quad (\text{A.7})$$

Multiplying both sides by $r^2 dr$ and integrating we get,

$$\int dr r^2 f(r) = \int \frac{dV}{4\pi} \nabla \cdot (\vec{B} B_r) \quad (\text{A.8})$$

Using Stokes theorem, the right hand side of the volume integral above can be expressed as a surface integral and hence,

$$\int dr r^2 f(r) = r^2 \int \frac{d\Omega}{4\pi} \hat{r} \cdot (\vec{B} B_r) \quad (\text{A.9})$$

Now, differentiating both sides w.r.t r we get:

$$f(r) = \frac{1}{r^2} \frac{d}{dr} (r^2 \langle B_r^2 \rangle) \quad (\text{A.10})$$

Using Eq (A.5), Eq (A.9) and the fact that $B^2 = B_r^2 + B_\theta^2 + B_\phi^2$, the expression for the angle-averaged radial force can be written as

$$4\pi \langle F_r \rangle = \frac{1}{2} \frac{d}{dr} [\langle B^2 \rangle - 2\langle B_r^2 \rangle] + \frac{2\langle B^2 \rangle - 3\langle B_r^2 \rangle}{r} \quad (\text{A.11})$$

The above expression for the angle-averaged radial Lorentz force can be simplified for some special magnetic field configurations which we enumerate below:

1. $\langle B_\theta^2 \rangle = \langle B_\phi^2 \rangle = 0$:

In this case, $\langle B^2 \rangle = \langle B_r^2 \rangle$. Hence

$$\langle F_r \rangle = -\frac{d}{dr} \left\langle \frac{B^2}{8\pi} \right\rangle - \frac{4}{r} \left\langle \frac{B^2}{8\pi} \right\rangle \quad (\text{A.12})$$

2. $\langle B_r^2 \rangle = \langle B_\theta^2 \rangle = \langle B_\phi^2 \rangle = \frac{1}{3} \langle B^2 \rangle$:

In this case, the simplified expression is,

$$\langle F_r \rangle = -\frac{1}{3} \frac{d}{dr} \left\langle \frac{B^2}{8\pi} \right\rangle \quad (\text{A.13})$$

References

- [1] N. Afshordi, R. Cen, *Astrophys. J.* **564** (2002) 669
- [2] N. Aghanim , S. Majumdar, J. Silk, *Repts. Prog. Phys.* **71** (2008) 066902
- [3] M. Arnaud , A. E. Evrard, *Mon. Not. Royal Astr Soc* **305** (1999) 631
- [4] M. Arnaud , 2005, astro-ph/0508159
- [5] Arshakian et al. , *Astron. Astrophys.* **494** (2009) 21
- [6] M. Birkinshaw, *Phys. Rept.* **310** (1999) 97
- [7] J. S. Bullock et al. , *Mon. Not. Royal Astr Soc* **321** (2001) 559
- [8] C. L. Carilli, G. B. Taylor, *Ann. Rev. Astron. & Astrophys.* **40** (2002) 319
- [9] Carlstrom et al. , 2009, arxiv:0907.4445
- [10] A. Cattaneo, R. Teyssier, *Mon. Not. Royal Astr Soc* **376** (2007) 1547
- [11] B. D. G Chandran, S. C. Cowley , *Phys. Rev. Lett.* **80** (1998) 3077
- [12] T. Chiueh, J-K Chou , *Astrophys. J.* **431** (1994) 380

- [13] Churazov et al. , *Astrophys. J.* **554** (2001) 261
- [14] T. E. Clarke , P. P. Kronberg, H. Böhringer , *Astrophys. J.* **547** (2001) L111
- [15] S. Colafrancesco, F. Giordano *Astron. Astrophys.* **454** (2006) L131
- [16] S. Cole, N. Kaiser, *Mon. Not. Royal Astr Soc* **233** (1988) 637
- [17] Dalla Vecchia et al. , *Mon. Not. Royal Astr Soc* **355** (2004) 995
- [18] K. S. Dawson et al. , *Astrophys. J.* **647** (2006) 13
- [19] Donahue et al. , *Astrophys. J.* **643** (2006) 730
- [20] K. Dolag , M. Bartelmann, H. Lesch , *Astron. Astrophys.* **387** (2002) 383
- [21] J. A. Eilek , F. N. Owen, 2002, *Astrophys. J.* **567** (2002) 202
- [22] S. Ettori, *Mon. Not. Royal Astr Soc* **344** (2003) L13
- [23] A. Finoguenov , T. H. Reiprich , H. Böhringer, *Astron. Astrophys.* **368** (2001) 749
- [24] A. Finoguenov , C. Jones, H. Böhringer , T. J. Ponman, *Astrophys. J.* **578** (2002) 74
- [25] Fixsen et al. , *Astrophys. J.* **473** (1996) 576
- [26] Golwala et al. , *Bull. Am. Astron. Soc.* **39** (2007) 886
- [27] S. F. Helsdon, T. J. Ponman , *Mon. Not. Royal Astr Soc* **315** (2000) 356
- [28] P. M. Koch , Puy D. Jetzer Ph, , 2003, *New. Astr.* **8** (2003) 1
- [29] E. Komatsu , U. Seljak , *Mon. Not. Royal Astr Soc* **336** (2002) 1256
- [30] E. Komatsu et al. , *Ap Jour. Supp* **180** (2009) 330
- [31] A. Kosowsky A., 2006, *New Astronomy Reviews*, 50, 969 *New. Astr Revs* **50** (2006) 969
- [32] D. Kushnir, B. Katz, E. Waxman, *Jour Cosm. AstroPart.* **9** (2009) 24
- [33] R. Lieu , J. P. D. Mittaz, S. N. Zhang, *Astrophys. J.* **648** (2004) 176
- [34] C. Loken , M. L. Norman , E. Nelson , G. L. Bryan, P. Motl , *Astrophys. J.* **579** (2002) 571
- [35] S. Majumdar S. 2008, *J.Phys : Conf. Ser.* 140 01200
- [36] M. Markevitch, *Astrophys. J.* **504** (1998) 27
- [37] T. Marriage, Atacama Cosmology Telescope Team, *Bull. Am. Astron. Soc.* **41** (2009) 755
- [38] Mathews et al. , 2004, *Astrophys. J.* **615** (2004) 662
- [39] I. G. McCarthy , A. Babul , M. L. Balogh, G. P. Holder, *Astrophys. J.* **591** (2003) 526
- [40] Mushotzky R. F., 2003, *AIP Conference Proceedings*, 666, 171
- [41] Myers et al. 2009, *Astro2010: The Astronomy and Astrophysics Decadal Survey*, Science White Papers, no. 218
- [42] R. Narayan, M. V. Medvedev , *Astrophys. J.* **562** (2001) L129
- [43] J. F. Navarro , C. S. Frenk, S. D. M. White, *Astrophys. J.* **462** (1996) 563
- [44] J. F. Navarro , C. S. Frenk, S. D. M. White, *Astrophys. J.* **490** (1997) 493

- [45] P. J. E. Peebles, *The Large Scale Structure of the Universe*, Princeton Univ. Press 1980, Princeton, NJ
- [46] R. Piffaretti, P. Jetzer , J. Kaastra, T. Tamura, *Astron. Astrophys.* **433** (2005) 101
- [47] Ponman et al. , *Nature* **397** (1999) 135
- [48] T. J. Ponman, A. J. R. Sanderson , A. Finoguenov, *Mon. Not. Royal Astr Soc* **343** (2003) 331
- [49] G. Pratt G., M. Arnaud, *Astron. Astrophys.* **408** (2003) 1
- [50] G. W. Pratt, M. Arnaud, E. Pointecouteau, *Astron. Astrophys.* **446** (2006) 429
- [51] W. H. Press, P. Schechter *Astrophys. J.* **187** (1974) 425
- [52] A. C. S. Readhead et al. *Astrophys. J.* **609** (2004) 498
- [53] C. L. Reichardt et al. *Astrophys. J.* **701** (2009) 1958
- [54] C. L. Reichardt et al. *Astrophys. J.* **694** (2009b) 1200
- [55] Roychowdhury et al. , *Mon. Not. Royal Astr Soc* **615** (2004) 681
- [56] Ruhl et al. , 2004, *Proc. SPIE.* **5498** (2004) 11
- [57] A. J. R. Sanderson, T. J. Ponman, A. Finoguenov, E. J. Lloyd-Davies , M. Markevitch, *Mon. Not. Royal Astr Soc* **340** (2003) 989
- [58] E. T. Scharlemann , *Astrophys. J.* **272** (1983) 279
- [59] Schleicher et al. 2009, *Astrophys. J.* **703** (2009) 1096
- [60] U. Seljak, K. M. Huffenberger, *Mon. Not. Royal Astr Soc* **340** (2003) 1199
- [61] J. L. Sievers et al. , [astro-ph/0901.4540](#)
- [62] Sunyaev R. & Zeldovich Y. B., 1970, *Comm. Astr. SpPhys.* **2** (1970) 66
- [63] Sunyaev R. & Zeldovich Y. B., 1972, Comments on Astrophysics and Space Physics, 4, 173
Comm. Astr. SpPhys **4** (1972) 173
- [64] G. B. Taylor, A. C. Fabian, S. W. Allen, *Mon. Not. Royal Astr Soc* **334** (2002) 769
- [65] A. Vikhlinin , M. Markevitch , S.S. Murray, *Astrophys. J.* **549** (2001) L47
- [66] M. G. Voit, *Rev. Mod. Phys.* **77** (2005) 207
- [67] P. Zhang , *Mon. Not. Royal Astr Soc* **348** (2004) 1348
- [68] Y. Zhang, X. Wu , *Astrophys. J.* **545** (2000) 141